Suomi-NPP VIIRS Surface Reflectance Algorithm Theoretical Basis Document (ATBD)

V1 Re-processing (NASA Land SIPS)

Principal Investigator: Dr. Eric F. Vermote

Correspondence e-mail address: Eric.F.Vermote@nasa.gov

Prepared by B. Franch, J. C. Roger and E. F. Vermote,

Version 2.0

October 10th 2016

Goddard Space Flight Center
Greenbelt, Maryland

Table of Contents

ATBD Outline for VIIRS Land Surface

1.0 INTRODUCTION

The algorithm described in this document produces the Surface Reflectance Intermediate Product (IP), one of over thirty products to be generated from the Visible/Infrared Imager/Radiometer Suite (VIIRS). The VIIRS prototype is carried onboard the NPOESS Preparatory Project (NPP) spacecraft launched by the National Aeronautics and Space Administration (NASA). The Surface Reflectance IP consists of directional surface reflectance values in bands centered at 0.412 μm, 0.445 μm, 0.488 μm, 0.555 μm, 0.645 μm, 0.672 μm, 0.865 μm (two different spatial resolutions), 1.24 μm, 1.61 μm (two different spatial resolutions), and 2.25 μm. It is an algorithm for surface reflectance retrieval that has been derived from Moderate Resolution Imaging Spectroradiometer.

The algorithm is designed to contain four modular components, namely, 'Extract inputs', 'Quality Flags', 'Surface Reflectance Retrieval', and 'Write Surface Reflectance IP'. The 'Surface Reflectance Retrieval' component consists of the Lambertian approximation/dynamic atmospheric adjustment, adjacency adjustment, and the bi-directional reflectance distribution function (BRDF) coupling adjustment. The 'Surface Reflectance Retrieval' component corrects for the effects of atmospheric gaseous absorption, molecular and aerosol scattering, thin cirrus contamination, glare from surrounding surface pixels (adjacency effects), and the coupling of the atmosphere and the surface bidirectional reflectance as a function of the viewing and solar geometries, elevation of the target and spectral band assuming a Lambertian surface. The atmospheric adjustment (within the 'Surface Reflectance Retrieval' component) includes 'near-real-time' updates of total column water vapor, ozone, and aerosol optical thickness data input fields. The surface reflectance values are subsequently corrected for adjacency and bi-directional reflectance distribution function (BRDF) effects. The aerosol information comes from the VIIRS Aerosol Optical Thickness IP. The total column water, column ozone, and surface pressure presently come from National Centers for Environmental Prediction (NCEP) feeds. Backup for water vapor comes from the VIIRS Precipitable Water and column ozone from the Ozone Mapping Profiling Suite (OMPS).

This document presents the theoretical basis of the Surface Reflectance IP algorithm. It is not meant to contain detailed information about the code design, the program data language, or code implementation. These details are given in the Operational Algorithm Description document (OAD) for this product or the VIIRS-NPP Surface Reflectance Users's guide.

1.1 Science/Applications Rationale for the Product

VIIRS spectral bands contain information about the sensor characteristics, the atmosphere, and primarily from the land surface. The sensor characteristics are generally

very well known, while the atmospheric characteristics are not as well known. Further, the atmospheric contribution to the at-satellite signal is much less than the land contribution, especially in most cloud-free conditions. Sensor and atmospheric effects need to be removed to retrieve the surface contribution. This result, usually expressed as a surface reflectance, may then be further refined to yield information useful to land remote sensing applications. The information derived from the surface reflectance and the VIIRS land EDRs could be used to study

- Effects of regional climate variations on agriculture, nutrient fluxes, and ecosystem stress;
- Agricultural and water resources management
- Climate change and weather prediction model outputs, and
- Soil moisture/boundary-layer interfacial parameterizations research, to name a few.

A number of VIIRS products require Surface Reflectance IP values as input. These include: top-of-atmosphere (TOA) and top-of-canopy (TOC) Enhanced Vegetation Index (EVI) and Normalized Difference Vegetation Index (NDVI); Surface Type; Surface Albedo; Soil Moisture; Snow Cover; Imagery for sea ice applications; and Sea Ice. Further, the products listed above feed into one another and into other VIIRS products, such as Leaf Area Index (LAI), and Active Fires. Hence, a need to derive an intermediate product (IP) for VIIRS that contains directional surface reflectance values for all relevant bands, and that accommodates the diverse requirements of the products that use it as input.

The VIIRS surface reflectance algorithm is based on a long heritage most recently coming from MODIS (Vermote et al., 1994; 1997; 2014; Vermote and Vermeulen, 1999). The spectral and spatial characteristics of the MODIS sensor are generally similar to the spectral and spatial requirements of the VIIRS sensor.

Operational implementation of the Surface Reflectance IP requires a hybrid approach using radiation transfer (RT) model-derived look-up tables (LUT) and a simple retrieval algorithm. The Second Simulation of the Satellite Signal in the Solar Spectrum (6S) first developed at the Laboratoire d'Optique Atmospherique of Lille, France, and then continuously improved for last 20 years at University of Maryland and NASA/GSFC (Vermote *et al.,* 1997; Vermote and Vermeulen, 1999; Kotchenova et al., 2006, 2007, 2008)) has been used to generate the VIRRS/LUTs.

1.2 Intended user community

The community is wide. It concerns all users involved or using surface reflectance products for studies in agriculture (Pinter et al., 1981; Tucker et al., 1983; Goward et al., 1987; Doraiswamy et al. 2005; Becker-Reshef et al., 2010; Meroni et al., 2013; Johnson, 2014; Franch et al., 2015), land cover change (Friedl et al., 2002; Friedl et al., 2010; Hansen & Loveland, 2012; Zhan et al., 2002) or even people working on surface characterization (Schaaf et al., 2002; Vermote, Justice, & Bréon, 2009). It is also one of

the inputs of some of the VIIRS official land products such as vegetation indexes, surface albedo, active fires detection and derived inputs from the surface reflectance.

2.0 THE ALGORITHM

2.1 Technical Background and Heritage

The Surface Reflectance IP algorithm is designed to contain four main subroutines: Extract inputs, Quality Flags, Surface Reflectance Retrieval and Write Surface Reflectance IP. The Surface Reflectance Retrieval subroutine is the main subroutine since it performs the lambertian approximation (atmospheric correction), the adjacency adjustment, and the bidirectional reflectance distribution function (BRDF) coupling adjustment.

The Surface Reflectance Retrieval routine corrects for the effects of gaseous absorption, molecular and aerosol scattering, thin cirrus contamination, glare from surrounding surface pixels (adjacency adjustment), and the coupling of the atmosphere and the surface bidirectional reflectance as a function of the viewing and solar geometries, elevation of the target and spectral band. The atmospheric adjustment (within the 'Surface Reflectance Retrieval' routine) includes updating the correction coefficients with 'in-view' total column water vapor, ozone, and aerosol optical thickness data input fields. The aerosol information required for surface reflectance retrieval comes from the VIIRS Aerosol Optical Thickness (AOT) IP and the Aerosol Model Information IP, complemented by total column water vapor, total column ozone, and surface pressure from National Centers for Environmental Prediction (NCEP) feeds. Backups for these inputs include total column ozone from the Ozone Mapping Profiling Suite (OMPS). The atmospherically corrected surface reflectance values derived using the Lambertian approximation are subsequently adjusted for adjacency and bi-directional reflectance distribution function (BRDF) effects. The BRDF-coupling adjustment is presently designed after the MODIS approach with a slight modification making the isotropic shape parameter a function of the normalized difference vegetation index, NDVI, (Vermote, 2003), an approximation due to operational constraints and the developmental maturity of the MODIS BRDF-coupling adjustment routine. The surface reflectance values after each adjustment are included as data layers in the surface reflectance IP along with the Land Quality Flags. The atmospheric inputs are available elsewhere, and the solar and viewing geometries are kept as part of the SDR.

Thin cirrus effects are removed by implementing an empirically based correction using VIIRS band M9 (1.38 μm). The quality control (QC) flags generated from the Build SDR module and the cloud and aerosol quality flag inputs are fused into a single Land Quality Flag (LQF) structure that applies to the Surface Reflectance IP, the Surface Albedo EDR, the Vegetation Index EDR, the Surface Type EDR. The LQF output is appended to the Surface Reflectance IP. Then the heart of the surface reflectance retrieval process begins, by converting the cirrus effects adjusted satellite reflectance values into surface reflectance values assuming the surface is Lambertian. The earth's

surface is generally not Lambertian, and as a result a further correction is applied. The conversion of the at-satellite-reflectance values to surface reflectance requires (i) the use of a set of conversion equations that also account for first order atmospheric multiple scattering effects, and (ii) inputs from pre-generated look up tables (LUTs) and analytic equations for gaseous or molecular effect.

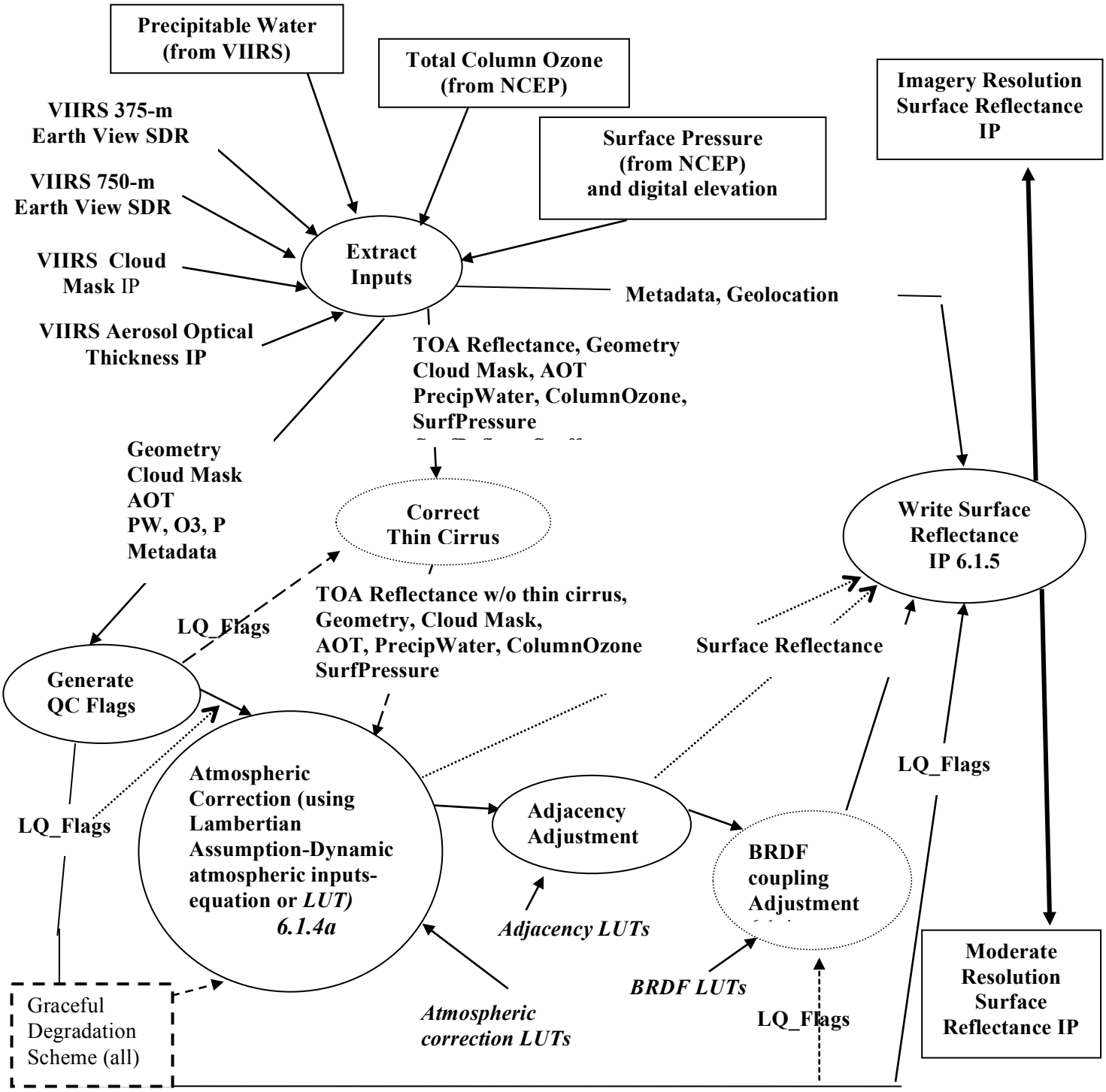

Figure 1. Surface Reflectance IP processing architecture.

The Lambertian surface reflectance value is passed simultaneously into the adjacency subroutine and to the 'write surface reflectance IP' routine. The output of the adjacency adjustment subroutine is simultaneously passed to the 'write surface reflectance IP' routine and to the BRDF-coupling adjustment subroutine. Some land quality (LQ) flags may be required during processing within the BRDF-coupling subroutine. The output of the BRDF–coupling adjustment routine is then passed to the 'write surface reflectance IP'.

2.2 Algorithm Description

2.2.1. Introduction

The retrieval of surface reflectance from electro-optical spectral sensors usually requires calibrating the sensor input to reflectance units, and removing the relatively small contribution due to the atmosphere. The principal atmospheric components affecting the top-of-atmosphere (TOA), or at-satellite-reflectance in the range of 0.4-2.5 μm are shown in Figure 2.

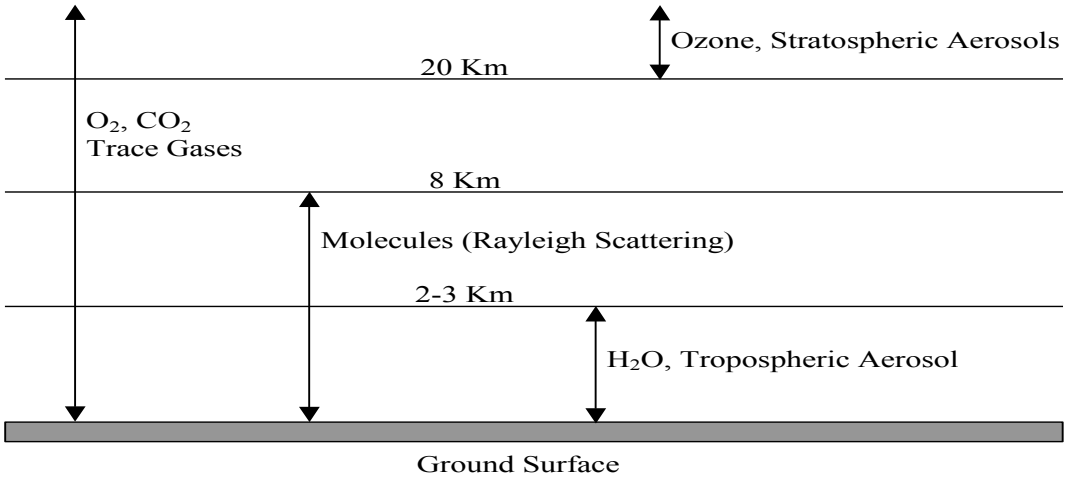

Figure 2. The atmospheric components affecting the remote sensing signal in the 0.4-2.5 μm range.

2.2.2 Lambertian correction

2.2.2.1 Formalism

Using the formalism developed for the 6S code, the solution of the radiation transfer equation employing the Lambertian Uniform Target assumption for observation in electro-optical spectral band i, assuming a standard atmospheric profile, but variable ozone and water vapor amount, is written as (Vermote *et al.*,1997):

$$\rho^i_{TOA}(\theta_s,\theta_v,\varphi,P,Aer^i,U_{H_2O},U_{O_3}) = Tg^i_{OG}(m,P)Tg^i_{O_3}(m,U_{U_{O_3}})[\rho^i_{atm}(\theta_s,\theta_v,\varphi,P,Aer^i,U_{H_2O})$$

$$+Tr^i_{atm}(\theta_s,\theta_v,P,Aer^i)\frac{\rho_s}{1-S^i_{atm}(P,Aer^i)\rho_s}Tg^i_{H_2O}(m,U_{U_{H_2O}})] \quad (1)$$

$$Aer^i = (\tau^i_A,\omega^i_0,P^i_A)$$

where (dropping the spectral dependence i)

ρ_{TOA} is the reflectance at the top of the atmosphere,
Tg is the gaseous transmittance by water vapor, Tg_{H_2O}, by ozone, Tg_{O_3}, or other gases, Tg_{OG} (e.g. CO_2, O_2, CH4)
Aer refers to the aerosol model optical properties,
ρ_{atm} is the atmosphere intrinsic reflectance,
Tr_{atm} is the total atmosphere transmission (downward and upward)
S_{atm} is the atmosphere spherical albedo,
ρ_S is the surface reflectance to be retrieved by the atmospheric correction procedure,

The geometrical conditions are given by θ_s, the solar zenith angle, θ_v, the view zenith angle and ϕ, the difference between the solar and view azimuth angle,

P is the pressure in Millibars, which influences the amount of molecules in the atmosphere and the concentration of absorbing gases,

τ_A, ω_0 and P_A describe the aerosol properties in band i.
τ_λ is the spectral aerosol optical thickness,
ω_0 is the spectral aerosol single scattering albedo, describing the absorption of the aerosol, ω_0 is equal to 1 for non-absorption particles and to 0 for completely absorbing aerosol,
P_A is the spectral aerosol phase function,

U_{H_2O} is the integrated water vapor content in centimeters
U_{O_3} is the integrated columnar ozone content in cm-atm
m is the air-mass computed as $1/\cos(\theta_s)+1/\cos(\theta_v)$

The water vapor affect on the atmosphere intrinsic reflectance is approximated in 6S as:

$$\rho^i_{atm}(\theta_s,\theta_v,\phi,P,Aer^i,U_{H_2O}) = \rho^i_R(\theta_s,\theta_v,\phi,P) +$$
$$\left(\rho^i_{R+Aer}(\theta_s,\theta_v,\phi,P,Aer^i) - \rho^i_R(\theta_s,\theta_v,\phi,P)\right)Tg^i_{H_2O}(m,\frac{U_{U_{H_2O}}}{2}) \quad (2)$$

where ρ_R represents the atmospheric reflectance due to molecular (Rayleigh) scattering, and ρ_{R+Aer} represents the reflectance of the combined molecular and aerosol components, which is computed in 6S using the successive order of scattering method, and thereby accounting correctly for the so-called coupling effect (Deschamps *et al*., 1983). This approximation conserves the correct computation of the coupling, and supposes that the

water vapor is mixed with aerosol and that the molecular scattering is not affected by the water vapor absorption. This approximation is reasonable in most cases where observation bands are narrow and outside the water vapor strong absorption as it is the case for VIIRS or MODIS.

The total atmosphere transmission, T_r, is further decomposed into downward and upward terms, which are respectively dependent on θ_s and θ_v and are computed using the same function by virtue of the reciprocity principle, that is:

$$Tr^i_{atm}(\theta_s, \theta_v, P, Aer^i) = T^i_{atm}(\theta_s, P, Aer^i)T^i_{atm}(\theta_v, P, Aer^i) \tag{3}$$

2.2.2.2 Lambertian infinite target correction implementation

In the implementation of the algorithm, functions related to atmospheric scattering and absorption, ρ_{atm}, T_{atm} and S_{atm} are interpolated from pre-computed look up table since they cannot be simply modeled. On the other hand, the gaseous transmission functions can be written as simple analytical expressions. The molecular reflectance term can be computed very efficiently using a semi-empirical approach based on the decomposition suggested by Chandrasekhar.

Using the approximation given below in (4), the dependence on the atmospheric pressure can be accounted for, by only computing ρ_{R+Aer} at standard pressure, P_0, which substantially reduces the dimension of the look-up tables. We use:

$$\begin{aligned}&\rho^i_{atm}(\theta_s, \theta_v, \phi, P, Aer^i, U_{H_2O}) = \rho^i_R(\theta_s, \theta_v, \phi, P) + \\ &\left(\rho^i_{R+Aer}(\theta_s, \theta_v, \phi, P_0, Aer^i) - \rho^i_R(\theta_s, \theta_v, \phi, P_0)\right)Tg^i_{H_2O}(m, \frac{U_{U_{H_2O}}}{2})\end{aligned} \tag{4}$$

A similar approach is applied to the atmospheric transmission term, that is:

$$T^i_{atm}(\theta, P, Aer^i) = T^i_{atm}(\theta, P_0, Aer^i)\frac{T^i_R(\theta, P)}{T^i_R(\theta, P_0)} \tag{5}$$

where T_R is the atmosphere transmission function due to molecule.

2.2.2.3 Lambertian infinite target correction operational approach

The code implements Equations (1) through (5), using a look-up table approach and analytic expressions. The following section details the computation of each term in the computer code.

2.2.2.3.1 Gaseous transmission by other gases

The gaseous transmission by gases, other than water vapor or ozone, $Tg^i_{OG}(m, P)$, in the VIIRS bands can written as a function of the air mass, m, and the pressure P (in atm), as follows:

$$Tg^i_{OG}(m,P) = \exp\left[m\left(a^i_0 P + a^i_1 Log(P)\right) + Log(m)\left(b^i_0 P + b^i_1 Log(P)\right) + mLog(m)\left(c^i_0 P + c^i_1 Log(P)\right)\right] \quad (6)$$

2.2.2.3.2 Ozone Gaseous transmission

The ozone gaseous transmission, $Tg^i_{O_3}(m,U_{O_3})$, in the narrow VIIRS bands (i.e., in the Chappuis band) could be simply modeled as:

$$Tg^i_{O_3}(m,U_{O_3}) = e^{-ma^i_{O_3}U_{o3}} \quad (7)$$

The coefficients $a_{O_3}{}^i$ are determined by curve fitting. The units of U_{O_3} are cm-atm.

2.2.2.3.3 Water vapor Gaseous transmission

The water vapor transmission, $Tg^i_{H_2O}(m,U_{H_2O})$, is modeled as:

$$Tg^i_{H_2O}(m,U_{H_2O}) = \exp\left[a^i_{H_2O} mU_{H_2O} + b^i_{H_2O} Log(mU_{H_2O}) + c^i_{H_2O} mU_{H_2O} Log(mU_{H_2O})\right] \quad (8)$$

The coefficients $a_{H2O}{}^i$, $b_{H2O}{}^i$ and $c_{H2O}{}^i$ are determined by curve fitting.

2.2.2.3.4 Molecular atmospheric reflectance at standard pressure

The molecular atmospheric reflectance at standard pressure, $\rho^i_R(\theta_s,\theta_v,\phi,P_0)$, is computed by the subroutine CHAND.f, which takes as input, the geometry (μ_s, μ_v, Φ), where μ_s (resp. μ_v) is the cosine of the solar (resp. view) zenith angle, and Φ the relative azimuth and the molecular optical thickness in that case at standard pressure, which is pre-computed (by 6S), τ_R.

2.2.2.3.5 Molecular atmospheric reflectance at actual pressure

The molecular atmospheric reflectance at actual pressure adjustment, $\rho^i_R(\theta_s,\theta_v,\phi,P_0)$, is simply done by adjusting the amount of molecule or the molecular optical thickness, according to:

$$\tau_R(P) = P\,\tau_R \quad (9)$$

where the pressure P is expressed in atmospheres.

2.2.2.3.6 Intrinsic reflectance at standard pressure

The intrinsic atmospheric reflectance at standard pressure, $\rho^i_{R+Aer}(\theta_s,\theta_v,\phi,P_0,Aer^i)$, is pre-computed by 6S in a look table for each band and each aerosol model (P_A,ω_0)) The step in solar zenith angle is 4 deg, in view angle is 4 deg

corresponding to the gauss quadrature of 24 angles (with the nadir added), the step is kept constant in scattering angle (4 degree), Θ, which is defined as:

$$\cos(\Theta) = -\cos(\theta_s)\cos(\theta_v) - \cos(\phi)\sin(\theta_s)\sin(\theta_v), \tag{10}$$

resulting in a variable number of steps for each θ_s, θ_v configuration. The indexing to the correct values in the look up table is achieved through the use of the ANGLE lookup table, which keeps track of the number of geometry computed for each θ_s, θ_v configuration. Though, more expensive and more complicated to interpolate within, this structure achieves a higher precision with a reduced size look up table, for a term whose accuracy is critical to the atmospheric correction.

The step in aerosol optical depth is variable to optimize the performance of the correction with the error induced by the interpolation (i.e. finer a low optical depth).

2.2.2.3.7 Atmospheric transmission on at standard pressure

Atmospheric transmission, $T_{atm}^{i}(\theta, P_0, Aer^{i})$, is pre-computed using 6S, with the successive order of scattering method assuming the bottom of the layer is illuminated with isotropic light. The code accounts for the mixing aerosol molecule within the atmosphere. The values are computed with a step of 4 deg in θ and for each aerosol model and each band for the predefined values of τ_A. The interpolation for any θ and τ is relatively straightforward since this table has only 2 dimensions. The table volume is also very modest.

2.2.2.3.8 Molecular (Rayleigh) transmission at standard pressure

The molecular transmission, $T_R^{i}(\theta, P_0)$, at standard pressure is computed using the value of molecular optical depth at standard pressure, τ_R. Using the two stream method, the molecular transmission is approximated by:

$$T_R^{i}(\theta, P_0) = \frac{\left\lfloor 2/3 + \cos(\theta) \right\rfloor + \left\lfloor 2/3 - \cos(\theta) \right\rfloor e^{-\tau_R / \cos(\theta)}}{4/3 + \tau_R} \tag{11}$$

2.2.2.3.9 Molecular (Rayleigh) transmission at actual pressure.

The Rayleigh transmission, $T_R^{i}(\theta, P)$, determination uses the same method as in Section 3.4.2.3.5 we simply replace τ_R in Equation (9) with $\tau_R(P)$.

2.2.2.3.10 Atmosphere spherical albedo at actual pressure

The atmospheric spherical albedo at actual pressure, $S_{atm}^{i}(P, Aer^{i})$, is defined as:

$$S_{atm}^{i}(P, Aer^{i}) = \int_0^{\pi/2} \int_0^{\pi/2} \int_0^{2\pi} \rho_{atm}^{i}(\theta, \theta', \phi, P, Aer^{i}) \sin(\theta)\cos(\theta') d\theta d\theta' d\phi \tag{12}$$

By ignoring the water vapor dependence on the atmosphere intrinsic reflectance (S acting as a second order effect), we can write the same relation we have written for the atmosphere intrinsic reflectance, that is

$$S^i_{atm}(P, Aer^i) = (S^i_{atm}(P_0, Aer^i) - S^i_R(P_0)) + S^i_R(P) \quad (13)$$

So the $S^i_{atm}(P_0, Aer^i)$ is stored in a pre-calculated look up table depending only on aerosol optical depth and model. The $S^i_R(P)$ term is computed by an analytic expression based on the integral of Equation (11) that is:

$$S^i_R(P) = \sum_j a_j EXPI(\tau_R, n) \quad (14)$$

where EXPI is the exponential integral function (see 6S code for details; Vermote et al., 1994).

2.2.3. Adjacency Adjustment

2.2.3.1. Formalism

If the target is of infinite dimension, the equation of transfer (here rewritten without gaseous absorption to simplify the writing), and dropping the spectral dependence then:

$$\rho_{toa} = \rho_{R+Aer} + \frac{T_{R+Aer}(\theta_s)T_{R+Aer}(\theta_v)\rho_s}{1 - S_{R+Aer}\rho_s} \quad (15)$$

In the case where the target is not infinite, Equation (15) becomes:

$$\rho_{toa} = \rho_{R+Aer} + \frac{T_{R+Aer}(\theta_s)}{1 - S_{R+Aer}\rho_e}\left(e^{-\tau/\mu_v}\rho_s + t^d_{R+Aer}(\theta_v)\rho_e\right) \quad (16)$$

$$\rho_e = \frac{1}{2\pi}\int_0^{2\pi}\int_0^{\infty}\rho(r,\psi)\frac{dF(r)}{dr}drd\psi \quad (17a)$$

In Equation (16), the downward transmission, $T_{R+Aer}(\theta_s)$, where θ_s refers to the solar zenith angle, and the upward transmission, $T_{R+Aer}(\theta_v)$, where θ_v refers to view zenith angle are considered separately. Furthermore, the upward transmission term, $T_{R+Aer}(\theta_v)$, is decomposed into two parts: (a) the diffuse upward transmission $t^d_{R+Aer}(\theta_v)$, and (b) the direct upward transmission ($e^{-\tau/\mu v}$), (where μ_v refers to the cosine of the view zenith angle and τ refers to the atmosphere optical thickness). In extenso, we have

$$T_{R+Aer}(\theta) = t^{d}_{R+Aer}(\theta) + e^{-\tau_{R+A}/\mu} \quad (17b)$$

By decomposing the signal in this way the contribution coming directly from the target the term ($e^{-\tau/\mu_v}\rho_s$) is isolated from the "environment contribution", ρ_e, coming from adjacent pixels not in the direct line of sight. The adjacent pixels contribute to the signal due to the atmospheric scattering of the photons toward the sensor and their contribution is therefore weighted by the diffuse upward transmission.

The effective "reflectance" of the environment, r_e, is not a simple average of the pixel around the target but is the result of the convolution of the atmospheric point spread function dF(r)/dr by the two dimensional surface reflectance values. In Equation (17), the spatial coordinate system used is the polar coordinate system (r for radius, Ψ for angle), which is very convenient since in most cases the point spread function is only dependent the distanced from the target and not the angle. In practice the dependence with respect to Ψ is actually dropped.

The atmospheric point spread functions for molecules and aerosols have been computed using Monte-Carlo computation and fitted using empirical functions and are available in the 6S code (Vermote et al., 1997). Figure 3 shows the environment function for molecules and aerosols as a function of the distance from the target center for nadir viewing condition and for a sensor located at the top of the atmosphere. In the aerosol case, the contribution of the environment decreases quickly with distance. In the case of molecules, scattering is more important, the contribution of the environment varies more slowly, and the impact of the environment can be seen at larger distances. It is worth pointing out that these environment functions will vary as a function of view angle and altitude of the sensor within the atmosphere (Vermote et al., 1997), and also, to a certain extent, will depend on the aerosol type (especially their vertical profile).

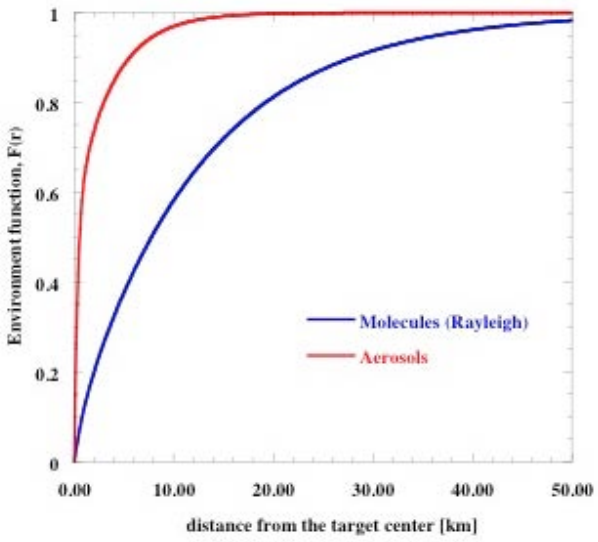

Figure 3: Atmospheric environment function as a function of the distance from the target center, for molecules and aerosols.

In practice, the atmosphere environment function, F(r), is computed by a weighting average of the individual molecules and aerosol environment functions using their respective upward diffuse transmissions,($t_d^R(\theta_v)$ and $t_d^{Aer}(\theta_v)$), that is:

$$F(r) = \frac{t_d^R(\theta_v)F^R(r) + t_d^{Aer}(\theta_v)F^A(r)}{t_d^{R+Aer}(\theta_v)} \tag{18}$$

2.2.3.2. Correction for adjacency effect-implementation

In the Lambertian approxiamtion, Equation (15) shows that the surface reflectance, ρ_{Lamb} can be retrieved in two simple steps given in Equation (19a) and (19b):

$$\gamma = \frac{\rho_{toa} - \rho_{R+Aer}}{T_{R+Aer}(\theta_s)T_{R+Aer}(\theta_v)} \tag{19a}$$

$$\rho_{Lamb} = \frac{\gamma}{1 + S_{R+Aer}\gamma} \tag{19b}$$

If the target is not of infinite radius then the result of Equation (19a), becomes,

$$\gamma = \frac{\rho_s e^{-\tau/\mu_v} + t_{R+Aer}^d(\theta_v)\rho_e}{T_{R+Aer}(\theta_v)\left(1 - S_{R+Aer}\rho_e\right)} \tag{20}$$

which can easily be solved for ρ_s:

$$\rho_s = [\gamma T_{R+Aer}(\theta_v)\left(1 - S_{R+Aer}\rho_e\right) - t_{R+Aer}^d(\theta_v)\rho_e] / e^{-\tau/\mu_v} \tag{21}$$

Since the Lambertian surface reflectance is computed before the adjacency correction (an average of the lambertian correction is needed in the adjacency correction) ρ_{Lamb} can be used instead of γ to compute ρ_s. This results in the following correction formula:

$$\rho_s = [\frac{\left(1 - S_{R+Aer}\rho_e\right)}{\left(1 - S_{R+Aer}\rho_{Lamb}\right)} T_{R+Aer}(\theta_v)\rho_{Lamb} - t_{R+Aer}^d(\theta_v)\rho_e] / e^{-\tau/\mu_v} \tag{22}$$

To compute r_e it is necessary to convolve the atmospheric point spread function with the two dimensional surface reflectance according to Equation (17a). The actual surface reflectance at a very fine scale level is usually not available; instead the actual measurements can be used. An approximation for Equation (17) (Putsay, 1992) is:

$$\rho_e = \sum_{j=-n}^{n}\sum_{i=-n}^{n} \frac{dF(r(i,j))}{dr}\rho_{Lamb}(i,j) \tag{23}$$

In Equation (23), the pixels of the image itself are used to compute the background reflectance, therefore the average point spread function at the pixel location (i,j) is used. The second approximation is that the estimate of the surface reflectance at

location (i,j) using the infinite radius target approximation is used instead of the actual reflectance. That provides a first guess for the environment contribution that may actually be refined by successive iterations, but those iterations are usually not necessary (Putsay, 1992).
This first guess is based on the order of tens to hundreds of pixels, which according to the MODIS surface reflectance ATBD corresponds to an n between 3 and 10. In practice, the contribution from the environment encompasses the pixels within 1200 m of the center pixel. The VIIRS algorithm uses n=3 for the imagery band values and n=2 for the moderate resolution band values.

2.3.3.3.Correction for adjacency effect-operational approach

Most of the term described in Equations (19) to (22) are already in look up table. The additional look up table that needs to be provided is the computation of the optical thickness at the given wavelenght, τ_{R+A}, used to compute the direct transmission term, $e^{-\tau_{R+A}/\mu_v}$, this optical thickness, $\tau_{R+A}=\tau_A+\tau_R$ is computed from the spectral extinction coefficient stored in the spherical albedo look up table to compute τ_A and the molecular optical thickness τ_R. The atmospheric point spread function is also stored as a look up table for the Rayleigh, $dF_R(r)/dr$ and aerosol contribution $dF_A(r)/dr$.

2.2.4 BRDF atmosphere coupling correction

2.2.4.1. Formalism

Equation (15) assumed that the target is lambertian, if we account for the fact that it is not a lambertian reflector, Equation (15) can be written as (Vermote, 1997)

$$\rho_{toa}(\mu_s,\mu_v,\varphi)=\rho_{R+Aer}(\mu_s,\mu_v,\varphi)+e^{-\tau/\mu_s}e^{-\tau/\mu_v}\rho_s(\mu_s,\mu_v,\varphi)+e^{-\tau/\mu_v}t_d(\mu_s)\overline{\rho}_s+e^{-\tau/\mu_s}t_d(\mu_v)\overline{\rho}'_s+$$
$$t_d(\mu_v)t_d(\mu_s)\overline{\overline{\rho}}_s+\frac{T_{R+Aer}(\mu_s)T_{R+Aer}(\mu_v)S_{R+A}\left(\overline{\overline{\rho}}_s\right)^2}{1-S_{R+Aer}\overline{\overline{\rho}}_s} \quad (23a)$$

with μ_s (resp. μ_v) the cosine of the sun (resp. view) zenith angle, ϕ the relative azimuth (sun – view), $\overline{\rho}_s$, $\overline{\rho}'_s$, and $\overline{\overline{\rho}}_s$ the term accounting for the coupling between the atmosphere and the surface BRDF, if the target is lambertian then $\overline{\rho}_s=\overline{\rho}'_s=\overline{\overline{\rho}}_s=r_s$; otherwise we have:

$$\overline{\rho}_s(\mu_s,\mu_v,\phi)=\frac{\int_0^{2\pi}\int_0^1\mu L^{\downarrow}_{R+A}(\mu_s,\mu,\phi')\rho_s(\mu,\mu_v,\phi'-\phi)d\mu d\phi'}{\int_0^{2\pi}\int_0^1\mu L^{\downarrow}_{R+A}(\mu_s,\mu,\phi')d\mu d\phi'} \quad (23b)$$

$$\overline{\rho}'_s(\mu_s,\mu_v,\phi)=\overline{\rho}_s(\mu_v,\mu_s,\phi) \quad (23c)$$

$$\overline{\overline{\rho}}_s(\mu_s,\mu_v,\phi)=\overline{\overline{\rho}'_s(\mu_s,\mu_v,\phi)} \quad (23d)$$

Where $L^{\downarrow}_{R+A}(\mu_s,\mu,\phi')$ is the downwelling flux.

Equation (23d) is approximated like the spherical albedo or white sky albedo, namely:

$$\overline{\overline{\rho}}_s \cong \int_0^1 \int_0^{2\pi} \int_0^1 \mu \rho_s(\mu, \mu, \phi' - \phi) d\mu d\phi' d\mu' \tag{23e}$$

2.2.4.2. BRDF atmosphere coupling correction Implementation

The BDRF of the target, $\rho_s(\mu, \mu', \phi')$ is in general unknown for any geometrical condition for the purpose of atmospheric correction. However, we will assume that the BRDF shape can be determined a priori. This simplifying assumption is necessary since Equation (23a) shows that the Top of the Atmosphere reflectance is given in terms of integrals of the BRDF of the surface Equations (23b-e). In other words Equation (23a) is a non-linear integral equation for the BRDF function. Solving this equation rigorously in an operational setting is prohibitive since it would require multiple iterations of a radiative transfer model.

The unknown reflectance is the line of sight reflectance $\rho_s(\mu_s, \mu_v, \phi)$ but the BRDF of the target $\rho_s(\mu, \mu', \phi')$ is assumed to satisfy:

$$\rho_s(\mu, \mu', \phi') = \rho_s(\mu_s, \mu_v, \phi) \frac{\rho_m(\mu, \mu', \phi')}{\rho_m(\mu_s, \mu_v, \phi)} \tag{24a}$$

Where $\rho_m(\mu, \mu', \phi')$ is the "modeled" BRDF and the ratio $\frac{\rho_m(\mu, \mu', \phi')}{\rho_m(\mu_s, \mu_v, \phi)}$ is the BDRF shape.

Using that assumption, Equation (23b) can be rewritten as:

$$\overline{\rho}_s(\mu_s, \mu_v, \phi) = \frac{\rho_s(\mu_s, \mu_v, \phi)}{\rho_m(\mu_s, \mu_v, \phi)} \overline{\rho}_m(\mu_s, \mu_v, \phi) = \rho_s(\mu_s, \mu_v, \phi) \overline{\rho}_m^{shape}(\mu_s, \mu_v, \phi) \tag{24b}$$

And similarly for Equations (23c) and (23e):

$$\overline{\rho}'_s(\mu_s, \mu_v, \phi) = \frac{\rho_s(\mu_s, \mu_v, \phi)}{\rho_m(\mu_s, \mu_v, \phi)} \overline{\rho}_m(\mu_v, \mu_s, \phi) = \rho_s(\mu_s, \mu_v, \phi) \overline{\rho}'^{shape}_m(\mu_s, \mu_v, \phi) \tag{24c}$$

$$\overline{\overline{\rho}}_s \cong \frac{\rho_s(\mu_s, \mu_v, \phi)}{\rho_m(\mu_s, \mu_v, \phi)} \int_0^1 \int_0^{2\pi} \int_0^1 \mu \rho_m(\mu, \mu', \phi' - \phi) d\mu d\phi' d\mu' = \rho_s(\mu_s, \mu_v, \phi) \overline{\overline{\rho_m^{shape}}}(\mu_s, \mu_v, \phi) \tag{24d}$$

So Equation (23a) is written as:

$$\rho_{toa}(\mu_s,\mu_v,\phi) = \rho_{R+Aer}(\mu_s,\mu_v,\phi) + \rho_s(\mu_s,\mu_v,\phi)[e^{-\tau/\mu_s}e^{-\tau/\mu_v} + e^{-\tau/\mu_s}t_d(\mu_v)\overline{\rho}_m^{shape}$$
$$+ e^{-\tau/\mu_s}t_d(\mu_v)\overline{\rho}_m'^{shape} + t_d(\mu_v)t_d(\mu_s)\overline{\overline{\rho}_m^{shape}}] + \rho_s(\mu_s,\mu_v,\phi)^2\frac{T_{R+Aer}(\mu_s)T_{R+Aer}(\mu_v)S_{R+Aer}\overline{\overline{\rho}_m^{shape}}^2}{1 - S_{R+Aer}\overline{\overline{\rho}_m^{shape}}} \quad (25)$$

Equation (25) is a quadratic equation in $\rho_s(\mu_s,\mu_v,\phi)$ that has only one positive solution, since the product of the roots is negative. Therefore solving for $\rho_s(\mu_s,\mu_v,\phi)$ is straightforward once each other term of Equation (25) is computed. The computation of $\overline{\rho}_m^{shape}$, $\overline{\rho}_m'^{shape}$ and $\overline{\overline{\rho}_m^{shape}}$, which are the only quantities not fully defined in the previous section, is described in the operational approach (next section).

2.2.4.3. BRDF atmosphere coupling correction-operational approach

The model of BRDF used for $\rho_m(\mu,\mu',\phi')$ is the operational model used for MODIS Albedo/BRDF product the LiSparse-Reciprocal (LSR), RossThick (RT) linear kernel model that is written as:

$$\rho_m(\mu_s,\mu_v,\phi) = P_1 + P_2K_{LSR}(\mu_s,\mu_v,\phi) + P_3K_{RT}(\mu_s,\mu_v,\phi) \quad (26)$$

where

$$K_{RT}(\mu_s,\mu_v,\phi) = \frac{(\pi/2 - \xi)\cos\xi + \sin\xi}{\mu_s + \mu_v} - \frac{\pi}{4}$$

$$\cos\xi = \mu_s\mu_v + \sqrt{1-\mu_s^2}\sqrt{1-\mu_v^2}\cos\phi$$

$$K_{LSR}(\mu_s,\mu_v,\phi) = O(\mu_s,\mu_v,\phi) - \frac{1}{\mu_s} - \frac{1}{\mu_v} + \frac{1}{2}(1+\cos\xi)\frac{1}{\mu_s}\frac{1}{\mu_v}$$

$$O(\mu_s,\mu_v,\phi) = \frac{1}{\pi}(t - \sin t\cos t)(\frac{1}{\mu_s} + \frac{1}{\mu_v})$$

$$\cos t = \frac{h}{b}\frac{\sqrt{D^2 + (\tan\theta'\tan\vartheta'\sin\phi)^2}}{\sec\theta' + \sec\vartheta'}$$

$$D = \sqrt{\tan^2\theta' + \tan^2\vartheta' - 2\tan\theta'\tan\vartheta'\cos\phi}$$

$$\theta' = \tan^{-1}(\frac{b}{r}\tan\theta_s) \qquad \vartheta' = \tan^{-1}(\frac{b}{r}\tan\vartheta_v)$$

where, h describes the crown model central height above the ground, r and b describe the vertical and horizontal dimensions of the crown spheroid.

The interesting properties of this BRDF model are that the geometrical conditions are decoupled from the surface weighting parameters, therefore:

$$\overline{\rho}_m^{shape}(\mu_s,\mu_v,\phi)=\frac{1+\frac{P_2}{P_1}\overline{K}_{LSR}(\mu_s,\mu_v,\phi)+\frac{P_3}{P_1}\overline{K}_{RT}(\mu_s,\mu_v,\phi)}{1+\frac{P_2}{P_1}K_{LSR}(\mu_s,\mu_v,\phi)+\frac{P_3}{P_1}K_{RT}(\mu_s,\mu_v,\phi)} \tag{27}$$

So by pre-computing the downward irradiance integrals $\overline{K}_{LSR}(\mu_s,\mu_v,\phi)$ and $\overline{K}_{RT}(\mu_s,\mu_v,\phi)$ for the kernels, $K_{LSR}(\mu_s,\mu_v,\phi)$ and $K_{RT}(\mu_s,\mu_v,\phi)$ storing them in look up tables (they are function of the band i, the optical thickness at 550nm, and the aerosol model), the functions $\overline{\rho}_m^{shape}(\mu_s,\mu_v,\phi)$ and their associate ($\overline{\rho}_m^{'shape}(\mu_s,\mu_v,\phi)$ and $\overline{\overline{\rho}}_m^{shape}$) can be recomputed on the fly. The only unknown at this point is the weight of the BRDF shape function, $P_2^{'}=\frac{P_2}{P_1}$ and $P_3^{'}=\frac{P_3}{P_1}$

Some experiments with MODIS data have shown that the BRDF shape parameter can be fitted as a function of NDVI. That is, to a first order, for low NDVI, low vegetation cover, P'_2 and P'_3 are expected to be near zero since the BDRF effect are small, for higher NDVI, the coefficient are expected to be higher. It should be noted, that P'_2 and P'_3 depend on the band as well. In the present version of the code, a linear interpolation is performed between a semi-arid case (low NDVI) and a forest case (high NDVI) for which the P'_2 are P'_3 have inverted using as large a data record as possible. Figure 4, shows the coefficients. P'_2 (Li Sparse Reciprocal) and P'_3 (Ross Thick) for three different biomass cases (low, average, high) for each of the VIIRS bands.

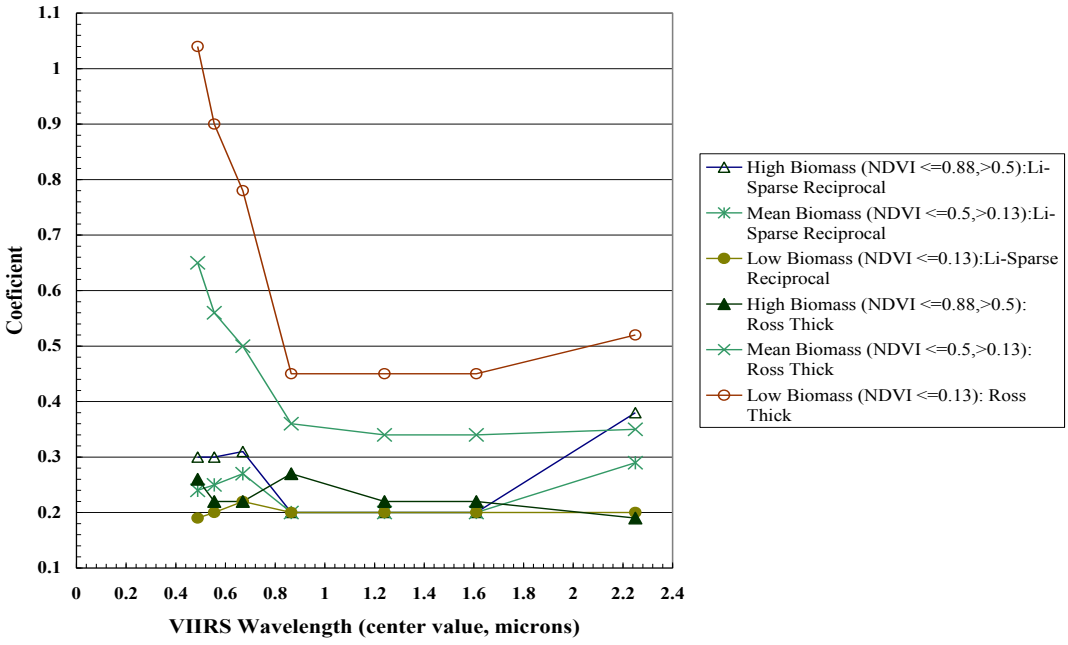

Figure 4. Relationship between BRDF shape and NDVI.

2.2.5 Thin Cirrus Correction

Should thin cirrus (presently defined to possess optical thickness at 640 nm ranging up to 1) be present, the Surface Reflectance IP and downstream products are generated, with an associated flag in the Land Quality Flag output. The baseline approach for removing much of the thin cirrus-laden pixels is very simple. It assumes that cirrus reflectance is not spectrally dependent, and that cirrus reflectance is spatially homogeneous. This allows the application of a threshold adjustment to all VIIRS bands in the general form

$$\rho_\lambda = \rho_\lambda - (\rho_{1.38} / T^{1.38}_{H20}) \quad (28)$$

where r_l is the reflectance at the particular band, $\rho_{1.38}$ is the reflectance at the 1.38 micron VIIRS band, and $T^{1.38}_{H20}$ is the total two-way transmittance of water vapor at 1.38 microns for the given solar and viewing geometry. $T^{1.38}_{H20}$ is assumed to be 0.6, based on Vermote and Vermeulen (1999).

This correction will be applied to the radiances in the other VIIRS reflective bands prior to the application of the lambertian correction. The inherent assumption within Equation (16), even at VIIRS scale, may not be valid under every circumstance, but suspected pixels are nonetheless flagged. A few reasons why the assumption might not be valid include, cirrus ice crystals are not spatially homogeneous, and cirrus adjacency issues. Vermote and Vermeulen (1999) provide additional insights.

2.3 Product Description

Most satellite data processing systems recognize five distinct levels of processing. Level 0 data is raw satellite feeds: level 1 data has been radiometrically calibrated, but not otherwise altered. Level 2 data is level 1 data that has been atmospherically corrected to yield a surface reflectance product. Level 3 data is level 2 data that has been gridded into a map projection, and usually has also been temporally composited or averaged. Level 4 data are products that have been put through additional processing. All data up to and including level 2 are in an ungridded orbital swath format, with each swath typically cut into small segments, or ***granules***, to facilitate processing. Data at level 3 and up are geolocated into a specific map projection, with the geolocated products typically in a set of non-overlapping ***tiles***.

The advantage of level 3 data over less processed forms of data is that each pixel of L3 data is precisly geolocated; a disadvantage is that the process of compositing or averaging that results in L3 data limits the usefulness of the L3 product. The Level 2G format, consisting of gridded Level 2 data, was developed as a means of separating geolocating from compositing and averaging. The L2G format preserves all the data that maps to a given pixel as observations at that pixel. Programs which produce level 3 data can then have all available data at each pixel to choose from, without having to geolocate everything themselves. An additional step of processing, level 2G-lite, provides a minimal level of compositing of daily level 2G data.

Surface reflectance for each pixel and for 12 bands (see Table 1) is obtained by adjusting top-of-atmosphere reflectance to compensate for atmospheric effects. Corrections are made for the effects of molecular gases, including ozone and water vapor, and for the effects of atmospheric aerosols. The inputs to the surface reflectance algorithm are top- of- atmosphere reflectances for the VIIRS visible bands (NPP_VMAE_L1, NPP_VIAE_L1), VIIRS cloud mask and aerosol products (NPP-CMIP_L2), aerosol optical thickness (NPP_VAOTIP_L2, NPP_VAMIP_L2), and atmospheric data obtained from a reanalysis (surface pressure, atmospheric precipitable water and ozone concentration).

Table 1. VIIRS bands included in Surface Reflectance products

Band Name[a]	Band center (μm)	Bandwidth[b] (μm)
M1	.415	.020
M2	.445	.018
M3	.490	.020
M4	.555	.020
I1	.640	.080
M5	.673	.020
I2	.865	.039
M7	.865	.039
M8	1.24	.020
I3	1.61	.060
M10	1.61	.060
M11	2.25	.050

[a] M indicates band with a nadir resolution of 750 m, I indicates band with a nadir resolution of 375 m.
[b] full width half maximum (FWHM)

The following surface reflectance products are generated at the Land SIPS: One Level 2 VIIRS surface reflectance product (VNP09), three Level 2G surface reflectance products (VNP09GA, VNP09G1KI, and VNP09GHKI), a global CMG-grid daily L3 surface reflectance (VNP09CMG), and two multi-day surface reflectance products (VNP09A1 and VNP09H1). See Table 2.

The L2 product, VNP09 and the daily L2G products VNP09GHK1 and VNP09G1KI are available from AS 5000 of LAADS (Level 1 and Atmosphere Archive and Distribution System, http://ladsweb.nascom.nasa.gov) only. VNP09 are available in the archive for all data days processed at SIPS, whereas the VNP09GHK1 and VNP09G1KI products from the last 40 data days are available online and the remaining days are only available on demand at LAADS-POD (Processing On Demand). The other products VNP09GA, VNP09A1, VNP09H1 and VNP09CMG are archived and distributed from both LAADS and LP-DAAC. (see "Suomi-NPP VIIRS surface Reflectance User's Guide V1 Re-processing", Roger et al., 2016).

Table 2. ***Land surface reflectance products produced by Land SIPS V1 reprocessing***

Products	ESDT	Description
Surface Reflectance (L2 Daily Swath product)	VNP09 *Available @LAADS*	VIIRS/NPP Surface Reflectance 5-Min Swath IP 375m and 750m Bands I1-I3, M1-M5, M7-M8, M10-M11. Output is in hdf 4 format
Surface Reflectance (L2G Daily Tiled products)	VNP09G1KI *Available for the latest 40 days @LAADS and for any prior days on demand @LAADS-POD*	VIIRS/NPP Surface Reflectance Daily L2G Global DDR 1km SIN Grid Day. Bands M1- M5, M7-M8, M10-M11. Input is VNP09 and output is in hdf 4 format
	VNP09GHKI *Available for the latest 40 days @LAADS and for any prior days on demand @LAADS-POD*	VIIRS/NPP Surface Reflectance Daily L2G Global DDR 500m SIN Grid Day. Bands I1- I3 Input is VNP09 and output is in hdf 4 format
	VNP09GA *Archived @LAADS and @LP_DAAC*	VIIRS/NPP Surface Reflectance Daily 1km and 500m L2G lite Bands I1- I3 (500m), Bands M1- M5, M7-M8, M10-M11 (1 Km) Inputs are VNP09G1KI and VNP09GHKI and output is in hdf5
Surface Reflectance (L3 8-day Composite Products)	VNP09A1 *Archived @LAADS and @LP_DAAC*	VIIRS/NPP 8-Day Surface Reflectance L3 1km SIN Grid. Bands M1- M5, M7-M8, M10-M11. Input is VNP09G1K1 and output is in hdf5
	VNP09H1 *Archived @LAADS and @LP_DAAC*	VIIRS/NPP 8-Day Surface Reflectance L3 500m SIN Grid. Bands I1- I3 Input is VNP09GHK1 and output is in hdf5
Surface Reflectance (L3 Daily CMG Products)	VNP09CMG *Archived @LAADS and @LP_DAAC*	VIIRS/NPP Daily Surface Reflectance L3 Global DDR 0.05°x0.05° grid CMG. Bands I1- I3, M1- M5, M7-M8, M10-M11 (M12-16 also added) Inputs are VNP09 and output is in hdf5

LAADS: Level 1 and Atmosphere Archive and Distribution System (https://ladsweb.nascom.nasa.gov)
LP_DAAC: Land Process Distributed Active Archive Center (https://lpdaac.usgs.gov)
POD: Processing On Demand

3.0 PRODUCT INPUTS

3.1 Spectral Bands

The Surface Reflectance IP algorithm uses the following VIIRS data:

- VIIRS Aerosol Optical Thickness IP
- VIIRS Precipitable Water IP (fallback water vapor source if it becomes available over land)
- VIIRS 375-m Earth View SDR (including radiances, geometry, geolocation, and elevation for bands I1, I2, and I3)
- VIIRS 750-m Earth View SDR (including radiances, geometry, geolocation, and elevation for bands M1, M2, M3, M4, M5, M7, M8, M10, and M11). The VIIRS M9 band is used for the cirrus correction.
- VIIRS Cloud Mask IP (including cloud and land/water mask)
- Surface Reflectance LUTs based on VIIRS spectral response curves

3.2 Masks, Thresholds and Ancillary Data

The Surface Reflectance IP algorithm uses the following non-VIIRS data:

- Surface Pressure from National Center for Environmental Prediction (NCEP), or Navy Operational Global Atmospheric Prediction System (NOGAPS) analyses, or a digital elevation map, such as the GTOPO05 from the EDC, USGS as a graceful degradation scheme.
- Precipitable Water from NCEP or NOGAPS analyses
- Column Ozone from NCEP or NOGAPS analyses
- Column Ozone from Ozone Mapping Profiling Suite (OMPS, fallback ozone source)

4.0 PRODUCT ACCURACCY /UNCERTAINTY

4.1 Uncertainty Estimate

The Surface Reflectance IP algorithm performance may be affected by sensor, solar and viewing geometry including target elevation above sea level, atmospheric, adjacency, and coupling of the atmosphere and surface effects, i.e. BRDF, among others. The atmospheric effects include aerosol and Rayleigh scattering, gaseous absorption, and thermodynamic conditions. The largest atmospheric effects on surface reflectance retrieval are from variations in aerosol properties. Sensor calibration is the primary contributor to sensor effects.

The effect of variations of input parameters on the surface reflectance calculated assuming a lambertian surface (r_l (lamb)), surface reflectance assuming a lambertian surface but adjusting for adjacency (r_l (adj)), as well as surface reflectance assuming a lambertian surface, adjusted for adjacency, and BRDF-coupling (r_l (BRDF)) can not be

investigated in detail until we obtain final sensor calibration curves, and additional vicarious calibration data cubes. Meanwhile a preliminary verification of the algorithm was performed on 2 scenes, and the results for a couple points within each scene are presented.

DERIVED REQUIREMENTS:

There are no explicit quality requirements on the Surface Reflectance IP in the VIIRS SRD. We have, however, derived performance requirements for surface reflectance retrievals to assist in the interpretation of our algorithm sensitivity tests. The requirements for surface reflectance are primarily derived from the specification requirements placed on the Vegetation Index Environmental Data Record (EDR), and the Surface Albedo EDR. The Surface Albedo EDR requires that the surface reflectance values be retrieved to within 0.05 of an albedo unit. For example, Liang et al. (2002) showed that when the surface reflectance values (derived from MODIS products) were within 5% absolute error, the resulting broadband albedo values had an absolute error within 2%. The Vegetation Index EDR has two general components, the Normalized Difference Vegetation Index (NDVI) and the Enhanced Vegetation Index (EVI). The implied specification on the top of canopy (TOC) EVI requires that in the most stringent case the VIIRS surface reflectance values be retrieved to within 0.012 of a surface reflectance unit. This would be sufficient to meet the specification on EVI but it is not necessary.

The absolute error in the retrieved surface reflectance assuming a lambertian surface is typically 0.02 to 0.06 of a unit for a clear atmosphere to 0.03-0.11 for a hazy atmosphere (aerosol optical thickness of 0.5) at a solar zenith angle of 60 degrees and at the maximum backscattering point (i.e., at the hot spot). Thus, in order to meet the system specification set for the vegetation index as well as the surface albedo, further adjustments are likely to be necessary. Lyapustin (2001) showed that as much as 0.04 – 0.06 absolute differences in the near infrared and 0.01-0.04 of a reflectance unit in the visible spectral range at a 25 m spatial resolution could be accounted for as the radiative contribution from surrounding pixels (not predominantly from the atmosphere), i.e., adjusting for adjacency effects. Adjacency adjustments are typically within 0.005 and 0.02 reflectance units at 1 km resolution. The assumption of a lambertian surface could contribute 0.02 – 0.06 reflectance units absolute difference (compared to true reflectance).

The current lack of sufficient data and final spectral response functions for VIIRS mandates that we perform a preliminary verification investigation of the VIIRS output against the corresponding output from MODIS despite their spectral and spatial differences. The result of this investigation requires a close agreement with the MODIS heritage sensor data, particularly in the VIIRS M4 and MODIS band 4 spectral region, where the spectral differences between the two sensors are minimal, in order for this algorithm to have a chance of meeting the derived requirements.

4.2 Validation Approach

Validation requires detailed knowledge of the relationship between processes and variables that may be used to monitor those processes over the full range of natural conditions. Pre-launch activities include determination of algorithms and characterization of uncertainties resulting from parameterizations and their algorithmic implementation. Post-launch activities include refinement of algorithms and uncertainty estimates based on near-direct comparisons with correlative data and selected, controlled analyses. The following provides a synopsis of the validation plan.

4.2.1 Pre-Launch Algorithm Test/Development Activities

Pre-launch algorithm and system performance validation will be performed primarily with MODIS data, as the spectral bands are very similar and in many cases identical to those for VIIRS. The algorithm heritage is also quite similar for the two systems. The MODIS validation infrastructure, combined with international cooperative efforts such as Long Term Ecological Research (LTER) and the Global Terrestrial Observing System (GTOS), will allow for rigorous validation without high cost or risk. Existing data sets have already played a role and will continue to do so; an example would be the AVHRR and Thematic Mapper (TM) data collected in the Boreal Ecosystem/Atmosphere Study (BOREAS) to retrieve surface reflectances. The atmospheric inputs can be obtained from *in situ* measurements made during the field campaigns such as BOREAS. Aerosol optical thickness (AOT) can be obtained from sun photometer observations made by the Aerosol Robotic Network (AERONET); the atmospheric conditions may be obtained from other *in situ* measurements or climatological data sets. By comparing those retrieved surface reflectance values with other multi-angular airborne measurements (Polarization and Directionality of the Earth's Reflectances [POLDER], Advanced Solid-state Array Spectroradiometer [ASAS]), Portable Apparatus for Rapid Acquisition of Bidirectional Observations of Land and Atmosphere (PARABOLA) measurements, and albedo measurements, we will address the accuracy, uncertainty, and precision of the retrieved surface reflectance values at different cases, e.g., their dependencies on the angular sampling, surface conditions, and seasonal changes (for example, snow and no-snow background conditions).

4.2.2 Post-Launch Algorithm Test/Development Activities

Post-launch algorithm and system performance validation/verification will exist as a continuation of the activities formulated and applied pre-launch. Focus will be placed on leveraging existing infrastructures for validation, not just from MODIS activities, but on a global scale. The validation at the sensor level can be accomplished by performing what is known as a vicarious calibration. A vicarious calibration campaign is concerned with the sensor, and seeks to determine the most representative value of at-satellite-radiance. It should be conducted over a bright surface (such as sand, snow), a dark surface (such as a densely vegetated forest, water body), a moderately dark, homogeneous, vegetated body, and a moderately dark, non-homogeneous, vegetated body. A vicarious calibration should, at the least, be conducted over both bright and dark surfaces. The degree of homogeneity varies according to the particular sensor spatial &

spectral properties as well as the solar & viewing geometries present during a particular overpass.

The requirements for a vicarious calibration are:

- A complete dataset to predict top of the atmosphere radiance.
  - A complete dataset is defined as containing sensor characteristics, and ground truth and atmospheric data. For example, surface reflectance, other biophysical data as necessary, surface BRDF, and atmospheric data
  - Data should be obtained for a view as consistent with the satellite-borne sensor being calibrated.
  - Data should be collected for similar solar/target geometry.
- Known sensor characteristics.
  - What are the gains and biases of the satellite sensor being calibrated?
  - What are the sources of error to the gains and biases?
  - An estimate of how well the surface features from course resolution environmental satellites match the location and extent of surface features observed at high spatial resolution over the measurement period, and one month time period.
- Knowledge of how well the surface feature maps match the ground observations
  - Do surface reflectance instrumentation have solar geometry module(s) similar to that of the satellite sensor being calibrated?
  - What are the accuracy and precision characteristics of the ground-truthing instrumentation
  - How many data points were obtained to represent the feature space?
  - How well do the data reproduce the feature space? (or how well did the sampling optimization scheme work?)
- A determination of the likelihood that "ground truth" on surface feature maps can be extracted from satellite data (i.e., VIIRS, ETM+, MODIS) in the desired region.

The optimal measurement collection conditions for a vicarious calibration are high elevation, homogeneous sites, when the sun is highest in the sky and the atmosphere is as blue as it can be. Less optimal conditions include data collection on thin overcast days. Thin overcast is defined as being able to see the cloud's disk through the cloud or haze layer. The data from these measurements could be useful, however. The data from these conditions since it could be instructive in comparison to optimal conditions. They will also provide a calibration and validation data to those developing cloud retrieval or QA/QC monitoring algorithms. Data collection should NOT occur on rainy days to prevent possible instrument damage from water and avoid the problems of impassable roads for example.

A likely instrumentation suite used in a vicarious calibration include a crop scan or preferably an ASD, sun photometer (or possibly shadow band radiometer), and GPS. An ASD is a hyper spectral version of the crop scan instrument. A ceptometer, fractional photosynthetic radiation (fPAR), and LAI-2000 sensors can be added if product

validation activities are combined with calibration activities. The latter should be a common practice for a number of reasons, the most important of which is economics.

A standard procedure for the field measurement component of a Vicarious Calibration begins like any other field measurement campaign, namely getting the instruments ready for field use. The field campaign locations will be determined according to need and programmatic requirements and are not considered here. Recall that multiple sampling locations might need to be sampled simultaneously. It may also be possible that these multiple sampling areas reside in different scenes, in which case the following has to be modified and applied to each location. One should try to get all locations simultaneously during the overpass of the sensor. This is not always possible due to instrumentation, personnel and other resource limitations. Keep in mind that it takes approximately 40 minutes to cover a nine-pixel area within a Landsat 7 image using a cropscan using one person. A nine-pixel area (or approx. 100 m by 100 m) should be large enough to estimate BRDF and adjacency effects for this 9-pixel area's center. This may or may not encompass enough points to reproduce all features in the satellite sensor's corresponding pixel or scene, which is one reason for sampling at ancillary sites.

One might employ a tool that determines the optimum way to cover the primary and ancillary target areas given the available resources. Such a tool would combine spectral information from operational satellite imagery at preferably better resolution than VIIRS, to create a coefficient of spectral variance to identify regions of relative homogeneity at various biomass levels (i.e. as low, middle, or high NDVI).

Each chosen area should be sampled in a pattern that is similar to, and at a spatial frequency that is at least double that of the imagery grid spacing. The latter is important in satisfying the last requirement of the vicarious calibration. Suffice it to say that this could mean that the sampling campaign becomes very labor intensive depending on the horizontal resolution of the satellite sensor's image. The tool could be applied to intensify or relax this sampling requirement, which is simply set in order to ensure that the ground truth observations can be used to derive the 'true' field of the parameter (process) they were meant to measure. The calibration/validation plan should provide additional details, which should vary as a function of the product that is to be validated, and possibly as a function of the sensor that is calibrated.

The sampling crews should consist of at least 3 people; One to operate the cropscan or ASD; one to operate a ceptometer (or other instrument); the third to operate the Microtops II (or other sun photometer), take notes and, if trained, to mark (given permission) the measurement points (at least with a GPS unit). There should not be any more than 4 people to a sampling crew unless there is instrumentation in addition to what has already been mentioned. A reduced crew size could be accommodated if measurements are made in the vicinity of existing field measurement infrastructure, such as the Oklahoma Mesonet, DOE ARM Cart site, or the USGS EDC 'instrumentation farm' (DeFelice, 2000; Crane and DeFelice, 2003; DeFelice et al. 2004).

5.0 DATA FORMAT

5.1 Format

Data are provided under hdf format. Table 3 gives the detail of layers for each product and exhaustive details can be found in the *"Suomi-NPP VIIRS surface Reflectance User's Guide V1 Re-processing", Roger et al., 2016*.

Table 3. Description of layer content for VIIRS SR product

VNP09 (16 layers)	375 m SR Band I1, 375 m SR Band I2, 375 m SR Band I3, 750 m SR Band M1, 750 m SR Band M2, 7 50 m SR Band M3, 750 m SR Band M4,750 m SR Band M5, 750 m SR Band M7, 750 m SR Band M8, 750 m SR Band M10, 750 m SR Band M11, SR Quality Flags 1*,* SR Quality Flags 2*,* SR Quality Flags 3, SR Quality Flags 4 SR Quality Flags 5*,* SR Quality Flags 6*,* SR Quality Flags 7
VNP09G1KI (36 layers)	1km SR M1 *first layer _1*, 1km SR M2 *first layer _1*, 1km SR M3 *first layer _1*, 1km SR M4 *first layer _1*, 1km SR M5 *first layer _1*, 1km SR M7 *first layer _1*, 1km SR M8 *first layer _1*, 1km SR M10 *first layer _1*, 1km SR M11 *first layer _1*, SR Quality Flags 1 *first layer _1*, SR Quality Flags 2 *first layer _1*, SR Quality Flags 3 *first layer _1*, SR Quality Flags 4 *first layer _1*, SR Quality Flags 5 *first layer _1*, SR Quality Flags 6 *first layer _1*, SR Quality Flags 7 *first layer _1*, Orbit and Coverage *first layer _1*, Number of observations, 1km SR M1 *compact layer _c*, 1km SR M2 *compact layer _c*, 1km SR M3 *compact layer _c*, 1km SR M4 *compact layer _c*, 1km SR M5 *compact layer _c*, 1km SR M7 *compact layer _c*, 1km SR M8 *compact layer _c*, 1km SR M10 *compact layer _c*, 1km SR M11 *compact layer _c*, SR Quality Flags 1 *compact layer _c ,* SR Quality Flags 2 *compact layer _c ,* SR Quality Flags 3 *compact layer _c,* SR Quality Flags 4 *compact layer _c,* SR Quality Flags 5 *compact layer _c,* SR Quality Flags 6 *compact layer _c,* SR Quality Flags 7 *compact layer _c,* Orbit and Coverage *compact layer _c*, Number of additional observations per row
VNP09GHKI (10 layers)	SR I1 *first layer _1*, SR I2 *first layer _1*, SR I3 *first layer _1*, Orbit and Coverage *first layer _1*, Number of observations, SR I1 *compact layer _c*, SR I2 *compact layer _c*, SR I3 *compact layer _c*, Orbit and Coverage *compact layer _c*, Number of additional observations per row
VNP09GA (58 layers)	Sensor Azimuth Angle *first layer _1*, Sensor Zenith Angle *first layer _1*, Solar Azimuth Angle *first layer _1*, Solar Zenith Angle *first layer _1*, SR M10 *first layer _1*, SR M11 *first layer _1* , SR M1 *first layer _1* , SR M2 *first layer _1*, SR M3 *first layer _1*, SR M4 *first layer _1*, SR M5 *first layer _1*, SR M7 *first layer _1*, SR

	M8 *first layer _1*, SR Quality Flags 1 *first layer _1*, SR Quality Flags 2 *first layer _1*, SR Quality Flags 3 *first layer _1*, SR Quality Flags 4 *first layer _1*, SR Quality Flags 5 *first layer _1*, SR Quality Flags 6 *first layer _1*, SR Quality Flags 7 *first layer _1*, Number of Observations 1 km *first layer _1*, Observations coverage 1km *first layer _1*, Orbit Pointer *first layer _1*, 500m SR I1*first layer _1*, 500m SR I2*first layer _1*, 500m SR I3*first layer _1*, Obs number of the corresponding obs at the coarser resolution *first layer _1*, Number of Observations 500 m, Observation coverage 500m *first layer _1*, Sensor Azimuth Angle *compact layer _c*, Sensor Zenith Angle *compact layer _c*, Solar Azimuth Angle compact layer _c, Solar Zenith Angle *compact layer _c*, 500m SR I1*compact layer _c*, 500m SR I2*compact layer _c*, 500m SR I3*compact layer _c*, SR M10 *compact layer _c*, SR M11 *compact layer _c*, SR M1 *compact layer _c*, SR M2 *compact layer _c*, SR M3 *compact layer _c*, SR M4 *compact layer _c*, SR M5 *compact layer _c*, SR M7 *compact layer _c*, SR M8 *compact layer _c*, SR Quality Flags 1 , SR Quality Flags 2 - *compact layer _c*, SR Quality Flags 3 - *compact layer _c*, SR Quality Flags 4 - *compact layer _c*, SR Quality Flags 5 - *compact layer _c*, SR Quality Flags 6 - *compact layer _c*, SR Quality Flags 7 - *compact layer _c*, Obs number of the corresponding obs at the coarser resolution *compact layer _1*, Number of additional observation in a row 1km, Number of additional observation in a row 500 m, Observations coverage 1km *compact layer _c*, Observation coverage 500m *compact layer _c*, Orbit Pointer *compact layer _c*
VNP09A1 (15 layers)	Relative Azimuth Angle, Sensor Zenith Angle, Solar Zenith Angle, Surface Reflect. Day of Year, SR M1, SR M10, SR M11, SR M2, SR M3, SR M4, SR M5, SR M7, SR M8, SR Band QC, SR State QA
VNP09H1 (5 layers)	SR Band I1, SR Band I2, SR Band I3, SR Band QC, SR State QA
VNP09CMG (33 layers)	Brightness Temperature Band M12, Brightness Temperature Band M13, Brightness Temperature Band M14, Brightness Temperature Band M15, Brightness Temperature Band M16, Granule Time, Number 375 m pixels averaged, Number 750 m pixels averaged, Number Mapping 1, Number Mapping 2 , Relative Azimuth Angle, Sensor Zenith Angle, Solar Zenith Angle, CMG SR State QA , SR Band I1, SR Band I2, SR Band I3, SR Band M1, SR Band M10, SR Band M11, SR Band M2, SR Band M3, SR Band M4, SR Band M5, SR Band M7, SR Band M8, SR Quality Flags 1, SR Quality Flags 2, SR Quality Flags 3, SR Quality Flags 4, SR Quality Flags 5, SR Quality Flags 6

5.2 QA Metadata

Operationally, quality control is automated for the Surface Reflectance IP, using the LQF output. These flags and their structure will be refined, as the development effort gets closer to launch readiness. The final structure likely contains a number of additional items more related to operational data transmission and processing (see *"Suomi-NPP VIIRS surface Reflectance User's Guide V1 Re-processing", Roger et al., 2016* for a description of Metadata).

6.0 PRODUCT PUBLICATIONS

Justice, C.O., Román, M.O., Csiszar, I., Vermote, E., Wolfe, R., Hook, S.J., Friedl, M., Wang, Z., Schaaf, C., Miura, T., Tschudi, M., Riggs, G., Hall, D.K., Lyapustin, A., Devadiga, S., Davidson, C., & Masuoka, E. (2013). Land and Cryosphere Products from Suomi NPP VIIRS: Overview and Status. Journal of Geophysical Research-Atmospheres, 118, 1-13, doi:10.1002/jgrd.50771.

Miura, T., Turner, J.P., & Huete, A.R. (2013). Spectral Compatibility of the NDVI Across VIIRS, MODIS, and AVHRR: An Analysis of Atmospheric Effects Using EO-1 Hyperion. IEEE Transactions on Geoscience and Remote Sensing, 51, 1349-1359, doi:10.1109/TGRS.2012.2224118.

Obata, K., Miura, T., Yoshioka, H., & Huete, A.R. (2013). Derivation of a MODIS-compatible enhanced vegetation index from visible infrared imaging radiometer suite spectral reflectances using vegetation isoline equations. Journal of Applied Remote Sensing, 7, 073467-073467, doi:10.1117/1.JRS.7.073467.

Vargas, M., Miura, T., & Shabanov, N. (2013). An Initial Assessment of the Suomi NPP VIIRS Vegetation Index EDR.Journal of Geophysical Research-Atmospheres, doi:10.1002/2013JD020439.

Vermote, E., Justice, C.O., Csiszar, I.A., (2014). Early evaluation of the VIIRS calibration, cloud mask and surface reflectance Earth data records, Volume 148, 25 May 2014, Pages 134-145. doi: 10.1016/j.rse.2014.03.028

Roger, J.C., Vermote, E., Devadiga, S, and Ray J.P. (2016) Suomi-NPP VIIRS Surface Reflectance User's Guide – V1 Re-processing (NASA land SIPS), Version 1.1, VIIRS document.

Wolfe, R.E., Lin, G., Nishihama, M., Tewari, K.P., Tilton, J.C., & Isaacman, A.R. (2013). Suomi NPP VIIRS prelaunch and on-orbit geometric calibration and characterization. Journal of Geophysical Research: Atmospheres,doi:10.1002/jgrd.50873

7.0 REFERENCES

Becker-Reshef I., Vermote E., Lindeman M., Justice C. 2010. A Generalized Regression-based Model for Forecasting Winter Wheat Yields in Kansas and Ukraine Using MODIS Data. Remote Sensing of Environment, 114, 1312-1323

Berk, A., G. P. Anderson, P. K. Acharya, J. H. Chetwynd, L. S. Bernstein, E. P. Shettle, M. W. Matthew, and S. M. Adler-Golden (1999). *MODTRAN4 User's Manual*. Air Force Research Laboratory, Space Vehicles Directorate, Hanscom AFB, MA 01731-3010.

Franch, B., Vermote, E.F., Becker-Reshef, I., Claverie, M., Huang, J., Zhang, J., Justice, C. and Sobrino, J.A. 2015. Improving timeliness of winter wheat production forecast in United States of America, Ukraine and China using MODIS data and NCAR Growing Degree Day. Remote Sensing of Environment, 161, 131-148.

Crane, M.P. and T.P. DeFelice, 2003. Enhancing the validation of remote Sensing data. AMS 12th SMOI, Long Beach, CA., 9-13 February, 001-001.

DeFelice, T.P., 2000. EDC Terrestrial-Ecosystem Assessment (TERESA) Site. Proc's USGS NMD Research Symposium, Apr. 25-27, Rolla, Missouri, 24-33.

DeFelice, T.P., and B.F. Wylie, 2001. Sky type discrimination using a ground based sunphotometer. *Atmos. Res.,* **59-60**, 313-329.

DeFelice, T.P., D. Lloyd, T.T. Baltzer, D.J. Meyer, P. Piraino, (2004). Water vapor correction of the daily 1-kilometer AVHRR global land dataset. Part I: Validation and use of the Water Vapor input field. *Int'l. J. Remote Sensing,* **24**(), 001-011.In Press.

Deschamps P.Y., Herman M., Tanre D, 1983, Modeling of the atmospheric effects and its application to the remote sensing of Ocean Color, *Applied Optics* , 22 (23): 3751-3758.

Doraiswamy, P. C. & P. W. Cook (1995) Spring wheat yield assessment using NOAA AVHRR data. Canadian Journal of Remote Sensing, 21, 43-51.

Friedl, M. ., McIver, D. ., Hodges, J. C. ., Zhang, X. ., Muchoney, D., Strahler, A., Schaaf, C. (2002). Global land cover mapping from MODIS: algorithms and early results. *Remote Sensing of Environment*, *83*(1-2), 287–302. http://doi.org/10.1016/S0034-4257(02)00078-0

Friedl, M. A., Sulla-Menashe, D., Tan, B., Schneider, A., Ramankutty, N., Sibley, A., & Huang, X. (2010). MODIS Collection 5 global land cover: Algorithm refinements and characterization of new datasets. Remote Sensing of Environment, 114(1), 168–182. http://doi.org/10.1016/j.rse.2009.08.016

Gao, B.-C., and Y.J. Kaufman (1993).. Water vapor retrieval from MODIS. In Vermote and Vermuelen (1998).

Hansen, M. C., & Loveland, T. R. (2012). A review of large area monitoring of land cover change using Landsat data. Remote Sensing of Environment, 122, 66–74. http://doi.org/10.1016/j.rse.2011.08.024

Hucks, J. (1998). VIIRS Testbed sensor modeling efforts, Phase I. Raytheon Systems Company Internal Memorandum Y1629.

IPO (2000). Visible/Infrared Imager/Radiometer Suite (VIIRS) Sensor Requirements Document (SRD) for National Polar-Orbiting Operational Environmental Satellite System (NPOESS) spacecraft and sensors, Rev. 3. Prepared by Assoc. Directorate for Acquisition, NPOESS Integrated Program Office, Silver Spring, MD.

Johnson, D. M. (2014). "An assessment of pre- and within-season remotely sensed variables for forecasting corn and soybean yields in the United States." Remote Sensing of Environment 141(0): 116-128.

Justice, C.O., E. Vermote, J.R.G. Townshend, R. DeFries, D.P. Roy, D.K. Hall, V.V. Salomonson, J.L. Privette, G. Riggs, A. Strahler, W. Lucht, R.B. Myneni, Y. Knjazikhin, S.W. Running, R.R. Nemani, Z. Wan, A.R. Huete, W. van Leeuwen, R.E. Wolfe, L. Giglio, J.-P. Muller, P. Lewis, and M.J. Barnsley (1998). The Moderate Resolution Imaging Spectroradiometer (MODIS): Land remote sensing for global change research, IEEE Trans. Geosci. Remote Sens., 36, 1228-1249.

Key, J. R., P. Yang, B. A. Baum, S. L. Nasiri (2000). Parameterization of shortwave ice cloud optical properties for various particle habits. Submitted to *Journal of Geophysical Research*.

Kneizys, F.X., L.W. Abreu, G.P. Anderson, J.H. Chetwynd, E.P. Shettle, A. Berk, L.S. Bernstein, D.C. Robertson, P. Acharya, L.S. Rothman, J.E.A. Selby, W.O. Gallery, and S.A. Clough (1996). *The MODTRAN 2/3 Report and LOWTRAN 7 Model*. L.W. Abreu and G.P. Anderson, eds. Prepared by Ontar Corporation, North Andover, Massachussets, for Phillips Laboratory, Geophysics Directorate, Hanscom AFB, Massachussets.

S.Y. Kotchenova, E.F. Vermote, R. Matarrese, & F.J. Klemm, Jr., Validation of a vector version of the 6S radiative transfer code for atmospheric correction of satellite data. Part I: Path radiance, *Applied Optics, Vol. 45, No. 26, p. 6762-6774., 2006*

S.Y. Kotchenova & E.F. Vermote, Validation of a vector version of the 6S radiative transfer code for atmospheric correction of satellite data. Part II: Homogeneous Lambertian and anisotropic surfaces, *Applied Optics, Vol. 46, No. 20, p. 4455-4464., 2007.*

S. Y. Kotchenova, E. F. Vermote, R. Levy, and A. Lyapustin, Radiative transfer codes for atmospheric correction and aerosol retrieval: intercomparison study, *Applied Optics, Vol. 47, No. 13, p. 2215-2226, 2008.*

Lee, T. Y., and Y. J. Kaufman (1986). Non-Lambertian effects on remote sensing of surface reflectance and vegetation index. *IEEE Transactions on Geoscience and Remote Sensing,* GE-24, 699-708.

Liang, S., others (2002). Validating MODIS land surface reflectance and albedo products: methods and preliminary results. *Remote Sensing of Environment*, **83** 001-014.

Lyapustin, A.I. (2001). Three-Dimensional Effects in the Remote Sensing of Surface Albedo. *IEEE Trans Geosci Remote Sens.,* Vol 39, 001-009.

Meroni, M.; Marinho, E.; Sghaier, N.; Verstrate, M.M.; Leo, O. Remote sensing based yield estimation in a stochastic framework—Case study of durum wheat in Tunisia. Remote Sens. 2013, 5, 539–557.

Pinter, P. J., R. D. Jackson, S. B. Idso & R. J. Reginato (1981) Multidate spectral reflectances as predictors of yield in water stressed wheat and barley. International Journal of Remote Sensing, 2, 43-48.

Running, S. W., C. Justice, V. Salomonson, D. Hall, J. Barker, Y. Kaufman, A. Strahler, A. Huete, J.-P. Muller, V. Vanderbilt, Z. M. Wan, P. Teillet and D. Carneggie (1994). Terrestrial remote sensing science and algorithms planned for EOS/MODIS. *Int. J. Rem. Sens.*, **15(17)**, 3587-3620

Schaaf, C. B., Gao, F., Strahler, A. H., Lucht, W., Li, X., Tsang, T., … Roy, D. (2002). First operational BRDF, albedo nadir reflectance products from MODIS. Remote Sensing of Environment, 83(1-2), 135–148. http://doi.org/10.1016/S0034-4257(02)00091-3

Tanré, D., B.N. Holben, and Y.J. Kaufman (1992). Atmospheric Correction algorithm for NOAA-AVHRR Products: Theory and Application. *IEEE Transaction on Geoscience and Remote Sensing*, **30**, 231-248.

Teillet, P.M. (1991). Radiometric and atmospheric correction procedures for AVHRR preprocessing in the solar reflective channels. *Proceedings of the Fifth International Colloquium on Measurements & Signatures in Remote Sensing, Courchevel, France,* Jan. 14-18, 101-104. Canada Centre Remote Sensing (CCRS) No. ESA-319; Remote Sensing on-line Retrieval System (RESORS) ID# 1083741. {Available from Author at CCRS, 588 Booth St., Ottawa, Ontario K1A 0Y7, Canada}.

Teillet, P.M. (1992). An algorithm for the radiometric and atmospheric correction of AVHRR data in the solar reflective channels. *Remote Sensing Environment,* **41**, 185-195.

Tucker, C. J., B. N. Holben, J. H. Elgin & J. E. McMurtrey (1980) Relationships of spectral data to grain yield variation. Photogrammetric Engineering and Remote Sensing, 46, 657-666.

Vermote, E.F. (2003). Adjacency effect. Encyclopedia of Optical Engineering, Marcel Dekker, Inc., NY, NY, 39-48.

Vermote, E.F., and A. Vermeulen (1999). Atmospheric correction algorithm: spectral reflectances (MOD09). Version 4.0. Algorithm technical background document. *NASA EOS-1D 2015 Doc.*

Vermote, E.F., D. Tanré, J.L. Deuzé, M. Herman, and J.J. Morrisette (1994). Second Simulation of the Satellite Signal in the Solar Spectrum (6S), 6S Version 0 User's Guide, April 18. *NASA Goddard Space Flight Center,* 183 pp.

Vermote, E.F., D. Tanré, J.L. Deuzé, M. Herman, and J.J. Morrisette (1997). Second Simulation of the Satellite Signal in the Solar Spectrum, 6S: An Overview. *IEEE Transactions on Geoscience and Remote Sensing,* 35, 675-686.

Vermote, E., Justice, C. O., & Bréon, F. M. (2009). Towards a generalized approach for correction of the BRDF effect in MODIS directional reflectances. IEEE Transactions on Geoscience and Remote Sensing, 47(3), 898–908. http://doi.org/10.1109/TGRS.2008.2005977

Vogelmann, J.E., and T.P. DeFelice (2003). Characterization of intra-annual reflectance properties of land cover classes in southeastern South Dakota using Landsat TM and ETM+ data. *Can. J. Remote Sens.* **29**(2), 219-229.

Zhan, X., Sohlberg, R. ., Townshend, J. R. ., DiMiceli, C., Carroll, M. ., Eastman, J., DeFries, R. . (2002). Detection of land cover changes using MODIS 250 m data. *Remote Sensing of Environment*, *83*(1-2), 336–350. http://doi.org/10.1016/S0034-4257(02)00081-0